

Enhanced thermoelectric performance of heavy-metals (M: Ba, Pb) doped misfit-layered ceramics: $(\text{Ca}_{2-x}\text{M}_x\text{CoO}_3)_{0.62}(\text{CoO}_2)$



Sajid Butt^{a,b}, Yaoyu Ren^a, Muhammad Umer Farooq^c, Bin Zhan^a, Rizwan Ur Rahman Sagar^d, Yuanhua Lin^a, Ce-Wen Nan^{a,*}

^a State Key Laboratory of New Ceramics and Fine Processing, School of Materials Science and Engineering, Tsinghua University, Beijing 100084, People's Republic of China

^b Department of Materials Science and Engineering, Institute of Space Technology, Islamabad 44000, Pakistan

^c School of Materials Science and Engineering, University of Science and Technology Beijing, Beijing 100083, People's Republic of China

^d Beijing National Center for Electron Microscopy, Beijing 100084, People's Republic of China

ARTICLE INFO

Article history:

Received 22 January 2014

Accepted 15 March 2014

Keywords:

Thermoelectric
 $(\text{Ca}_2\text{CoO}_3)_{0.62}(\text{CoO}_2)$
Layered ceramic
SPS

ABSTRACT

We present the temperature dependent thermoelectric properties of polycrystalline misfit-layered ceramics; $(\text{Ca}_{2-x}\text{M}_x\text{CoO}_3)_{0.62}(\text{CoO}_2)$ (M: Ba and Pb, $x = 0, 0.1, 0.2$), fabricated by sol–gel method followed by spark plasma sintering technique. The X-ray diffraction results confirmed the substitution of Ba and Pb in the lattice of $(\text{Ca}_2\text{CoO}_3)_{0.62}(\text{CoO}_2)$ at Ca-site. An improved grain-alignment was observed at small scale with Ba-doping, which helped increasing the electrical conductivity but for the Pb-doped specimens, the electrical conductivity was suppressed by catastrophic grain-alignment. The bivalent metallic-doping induced a spin-entropy enhancement which resulted in an enhanced thermopower. For Ba-doped specimens, the simultaneous increase in the electrical conductivity and the thermopower resulted in an increased power factor exhibiting the highest value of $527 \mu\text{W}/\text{mK}^2$. On the other hand, Pb-doping increased the thermopower but on the expense of electrical conductivity. Although, Pb-doping decreased the electrical conductivity but on the other hand, the enhanced thermopower and the suppressed thermal conductivity were sufficient for achieving ZT value higher than that of pure $(\text{Ca}_2\text{CoO}_3)_{0.62}(\text{CoO}_2)$. Among all the pure and doped samples, the highest ZT value of ~ 0.33 at 1000 K was achieved by Ba-doping which is about 100% higher than that of the pure $(\text{Ca}_2\text{CoO}_3)_{0.62}(\text{CoO}_2)$.

© 2014 Elsevier Ltd. All rights reserved.

1. Introduction

Today about 90% of the world's electricity demand is met by the burning fossil fuels in heat engines operating at an average conversion efficiency less than 50%, thus about 15 terawatts of energy is escaped to the environment as heat losses [1,2]. Thermoelectric (TE) devices are the potential candidate for recovering a part of this waste heat directly into electricity without any mechanical part [3,4]. The recovery performance of a TE material is determined by a dimensionless figure-of-merit: $ZT = (\sigma S^2/k)T$, where σ , S , T and k are the electrical conductivity, thermopower, working-temperature and the thermal conductivity, respectively [5]. Therefore, a good TE material must possess higher the electrical conductivity and thermopower but smaller the thermal conductivity.

The oxide TE materials are the future of thermoelectricity owing to their non-toxicity and environment friendliness. Among the oxide TE materials, BiCuSeO have attracted much attention due to

its higher ZT value [6,7]. Unlike traditional TE oxide materials [8–10], it can only be synthesized in strict stoichiometric oxygen ambient which makes its preparation more expensive and harder than that of traditional TE oxide materials. On the other hand, easier and cheaper synthesis route for $\text{Na}_x\text{Co}_2\text{O}_4$ [8], $\text{Ca}_3\text{Co}_4\text{O}_9$ (CCO) embodied as $(\text{Ca}_2\text{CoO}_3)_{0.62}(\text{CoO}_2)$ [9] and $\text{Bi}_2\text{Sr}_2\text{Co}_2\text{O}_x$ [10] has made layered cobaltite an attractive candidate for high temperature TE applications. Among these cobaltites, the misfit layered $(\text{Ca}_2\text{CoO}_3)_{0.62}(\text{CoO}_2)$ is regarded as a promising TE material because of strong electronic correlation and chemically stability at higher temperatures [11–13]. It is composed of two alternate subsystems; one with triple rock salt-type Ca_2CoO_3 (RS) layers and the other with CdI₂-type CoO_2 layers. The subsystems are stacked along c-axis having same lattice parameter a , c and β parameter, but the different lattice parameter b makes it a misfit structure along b -axis. The RS Ca_2CoO_3 layer is regarded as an insulating media which maintains the charge supply for the conducting CoO_2 layer [9]. The ZT value for a single crystalline CCO has been reported to be reaching 1 at 1000 K [14], making it a promising p-type TE material to be investigated further. However, ZT for a polycrystalline

* Corresponding author.

E-mail address: cwnan@tsinghua.edu.cn (C.-W. Nan).

CCO is still lower and many reports have addressed an elemental doping at Ca-site [12,15–27], Co-site [28–33] and the dual doping: both at Ca-site and Co-site [34–36] for improving the TE performance. In the CoO_2 layers, Co is found to exist as Co^{+3} and Co^{+4} ions [9]. Tang et al. reported that the rare earth elemental doping at Ca-site could effectively suppress Co^{+4} concentration, resulting in a spin-entropy enhancement which is a likely source of high thermopower in cobaltates [17]. Zhang et al. [25] and Lu et al. [26] have reported that the Ba doping at Ca-site in CCO improved TE properties, resulted from the suppressed electrical resistivity and the thermal conductivity without any increase in the thermopower. Nakatsugawa et al. [27] have discussed the partial substitution of Pb at Ca-site in CCO at low temperatures – it was suggested that Pb doping could not show adequate improvements in the electrical conductivity and the thermopower at low temperatures.

In the present work, we have discussed the high temperature TE properties of heavy-metals doped misfit-layered $(\text{Ca}_{2-x}\text{M}_x\text{CoO}_3)_{0.62}$ (CoO_2); (M: Ba and Pb, $x = 0, 0.1, 0.2$) ceramics. For Ba-doped CCO, a clear contradiction with Ref. [25,26], we have obtained a simultaneous increase in the electrical conductivity and the thermopower. However, for Pb-doping, the TE properties were improved because of an increased thermopower and the suppressed thermal conductivity at higher temperatures which contradicted the results reported in Ref. [27]. In addition, we have investigated and discussed the spin-entropy enhancement as an origin of improved thermopower for the Ba- and Pb-doped CCO.

2. Experimental

Sol-gel method as described below, was used to synthesis a series of pure and doped $(\text{Ca}_{2-x}\text{M}_x\text{CoO}_3)_{0.62}$ (CoO_2) ceramics; (M: Ba and Pb, $x = 0, 0.1, 0.2$). The stoichiometric amounts of $\text{Ca}(\text{NO}_3)_2 \cdot 4\text{H}_2\text{O}$, $\text{Co}(\text{NO}_3)_2 \cdot 6\text{H}_2\text{O}$, $\text{Pb}(\text{NO}_3)_2$, $\text{Ba}(\text{NO}_3)_2$ and citric acid monohydrate (molar ratio: citric acid/metal cations ≈ 1.5) as a chelating agent were used as the starting reagents for preparing the two different series of $(\text{Ca}_{2-x}\text{Ba}_x\text{CoO}_3)_{0.62}$ (CoO_2) and $(\text{Ca}_{2-x}\text{Pb}_x\text{CoO}_3)_{0.62}$ (CoO_2); ($x = 0, 0.1, 0.2$). Stoichiometric mixtures of metal salts and citric acid were thoroughly mixed in the distilled water and continuously stirred at 80°C for 3 h. The obtained homogenous solutions were dried at 130°C for 12 h. Dried spongy gels were crushed and then calcined at 800°C for 4 h in the air. Upon calcination, the metallic nitrates are converted to their respective metallic oxides. While raising the calcination temperature above 600°C , CaO and Co_3O_4 start to be crystallized into CCO and the reaction is completed at 772°C [37]. The obtained black agglomerated powders were grounded and sintered by spark plasma sintering (SPS; DR. SINTER MULTI). For SPS, the powdered material was put into a graphite die having a diameter of 20 mm, lined internally with a graphite foil. This assembly was heated gradually up to 750°C in the vacuum and kept at this temperature for 5 min under a pressure of 50 MPa. After cooling to room temperature, the obtained pellets were annealed at 750°C in the air for the removal of carbon over the surface.

The crystal structure was analyzed with the help of X-ray diffraction (XRD) data collected by Rigaku X-ray Diffractometer by using $\text{Cu K}\alpha$ ($\lambda = 0.15406 \text{ nm}$) radiations. The effects of doping on the chemical state of Co were investigated with X-ray photoelectron spectroscopy: (XPS Escalab-250xi). The grain morphology was examined by a field-emission scanning electron microscope (SEM: Jeol-jsm7001f). The thermal conductivity k was measured by the formula i.e.; $k = DC_p d$, where D is the thermal diffusivity and C_p is the specific heat, simultaneously measured by Laser Flash method (Netzsch LFA 457) and d is the mass density given by Archimedes principle. The DC electrical conductivity was calculated from van der Pauw method and thermopower was evaluated from slope of the graph for potential difference vs.

temperature difference, with the help of a computerized home-made apparatus.

3. Results and discussion

3.1. Structural analysis

The XRD patterns for all the pure and doped sintered specimens, obtained from the surface perpendicular to the pressure axis, are shown in Fig. 1. The diffraction peaks in all the pure and doped specimens represent polycrystalline CCO crystal structure, verified by PDF# 21-0139 with an exception of few low intensity diffraction peaks appeared in the doped samples, as shown in Fig. 1. XRD pattern of all the specimens showed strong diffraction lines along (001) plane, which inferred that the preferential site of growth lied in the c -axis direction for the samples compacted by SPS technique.

The lattice parameters and the β^0 parameter were calculated from the peak-positions attributed to the experimental data shown in Fig. 1, and the (hkl) indices reported in Ref. [9]. The systematic change in the lattice parameters of doped specimens (given Table 1) affirms the substitution of metallic ions; Ba^{2+} and Pb^{2+} into the parent lattice of CCO.

3.2. Morphological properties

The SEM micrographs of fractured cross-sectional view of selected samples are shown in Fig. 2. With SPS, the dense micrograins having a lamellar structure have been grown particularly for pure and Ba-doped specimens, as shown in Fig. 2(a and b). For the Ba-doped specimens, it can be observed that the grains have become flatten and larger in size as compared to pure CCO shown in Fig. 2(b). Thus, the number of grain boundaries was decreased with an improved grain-alignment at the small scale, which would aid the transportation of carriers by minimizing the scattering from grain boundaries. On the other hand, Fig. 2(c) clearly demonstrates that the Pb-doping disrupts the grain-alignment which would result in an increased carrier scattering with grain boundaries.

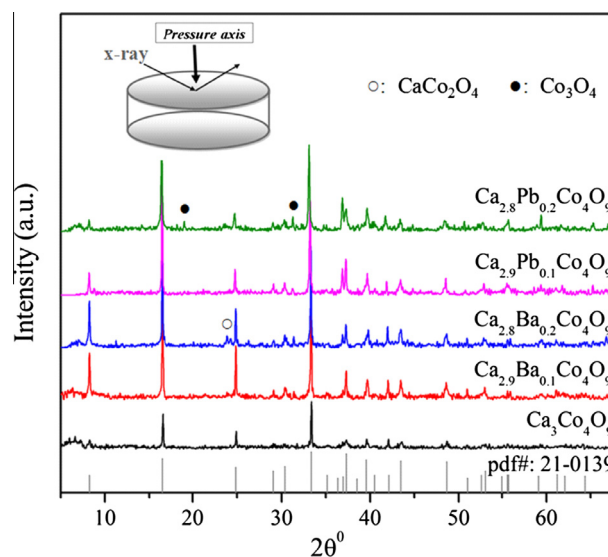
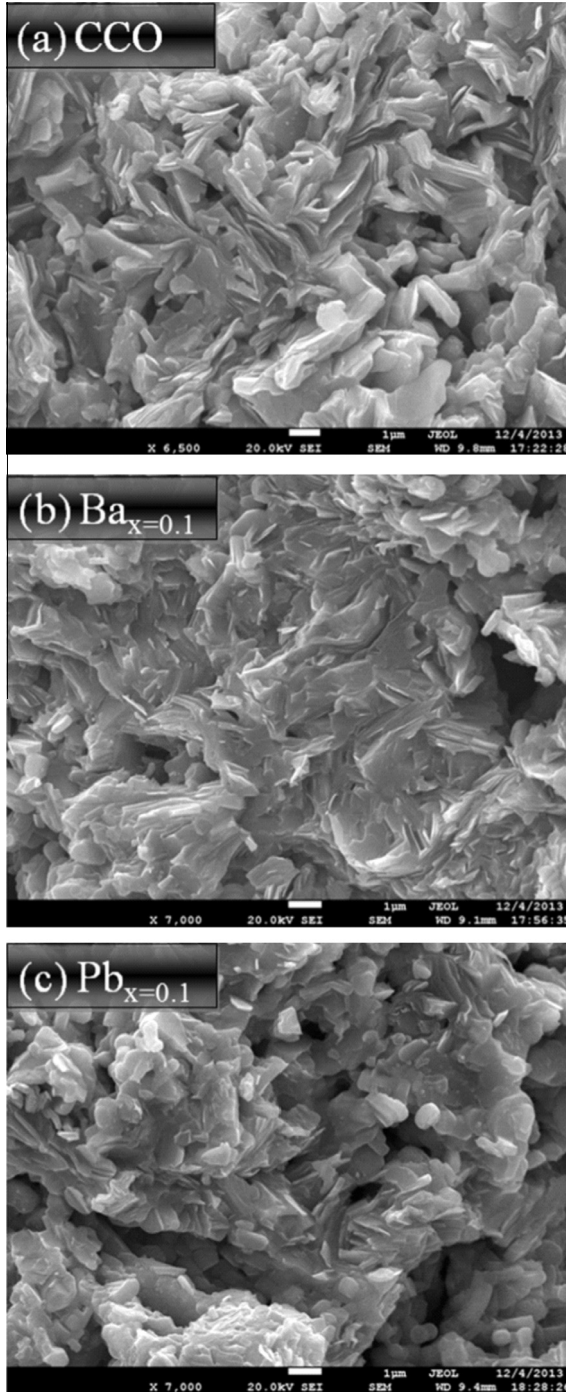


Fig. 1. XRD patterns of pure and doped $(\text{Ca}_{2-x}\text{M}_x\text{CoO}_3)_{0.62}$ (CoO_2); (M: Ba and Pb) ceramics. The line pattern in the bottom represents JCPDS (PDF # 21-0139) for pure phase of $\text{Ca}_3\text{Co}_4\text{O}_9$.

Table 1

Chemical compositions and cell parameters determined from XRD data.

| Composition | Abbreviation | a (Å) | b_1 (Å) | c (Å) | β° |
|---|---------------------|---------|-----------|---------|---------------|
| $(\text{Ca}_2\text{CoO}_3)_{0.62}(\text{CoO}_2)$ | CCO | 4.825 | 4.544 | 10.831 | 98.2 |
| $(\text{Ca}_{1.9}\text{Ba}_{0.1}\text{CoO}_3)_{0.62}(\text{CoO}_2)$ | $\text{Ba}_x = 0.1$ | 4.832 | 4.538 | 10.845 | 98.0 |
| $(\text{Ca}_{1.8}\text{Ba}_{0.2}\text{CoO}_3)_{0.62}(\text{CoO}_2)$ | $\text{Ba}_x = 0.2$ | 4.836 | 4.527 | 10.856 | 98.0 |
| $(\text{Ca}_{1.9}\text{Pb}_{0.1}\text{CoO}_3)_{0.62}(\text{CoO}_2)$ | $\text{Pb}_x = 0.1$ | 4.836 | 4.540 | 10.890 | 98.2 |
| $(\text{Ca}_{1.8}\text{Pb}_{0.2}\text{CoO}_3)_{0.62}(\text{CoO}_2)$ | $\text{Pb}_x = 0.2$ | 4.833 | 4.542 | 10.907 | 99.1 |

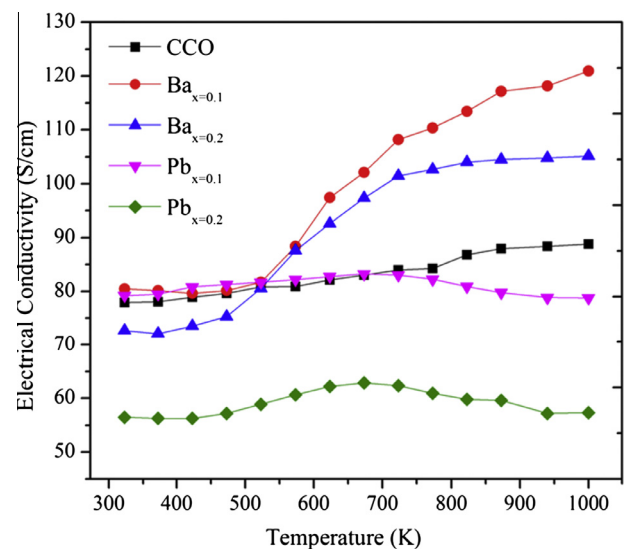
**Fig. 2.** The SEM micrographs of fractured cross-sectional view of selected samples sintered by SPS (a) $(\text{Ca}_2\text{CoO}_3)_{0.62}(\text{CoO}_2)$, (b) $(\text{Ca}_{1.9}\text{Ba}_{0.1}\text{CoO}_3)_{0.62}(\text{CoO}_2)$ and (c) $(\text{Ca}_{1.9}\text{Pb}_{0.1}\text{CoO}_3)_{0.62}(\text{CoO}_2)$.

3.3. Thermoelectric transport properties

The temperature dependence of the electrical conductivity, thermopower and the thermal conductivity was investigated from 323 K to 1000 K for determining the thermoelectric transportation in pure and doped specimens.

Fig. 3 presents the temperature dependence of electrical conductivity for pure and doped specimens from 323 K to 1000 K. The electrical conductivity for all the pure and Ba-doped series was increased with an increasing temperature which marked a typical semiconducting behavior. A sudden increase in the conductivity can be observed around 550 K, particularly for Ba-doped specimens, as shown in Fig. 3. This increase in the conductivity is associated with the spin-state transition of Co [9].

An evident increase in the electrical conductivity can be seen with Ba-doping specifically at higher temperatures and the highest value of 121 S/cm among all the pure and doped specimens was achieved by $\text{Ba}_x = 0.1$. The improvement in the electrical conductivity can be associated with the improved grain-alignment induced by Ba-doping, as discussed above in the morphology section, and a difference in the electronegativities of Ca- and Ba-ions. Upon further increase in the Ba-doping contents ($x > 0.1$), the electrical conductivity was decreased because the heavy doping concentration might increase the carrier's scattering to result in a decreased electrical conductivity [25]. On the other hand, Pb-doping could not bring any improvement in the electrical conductivity. For the Pb-doped series, a hump like shape was obtained for the temperature dependence of electrical conductivity, as shown in Fig. 3. It can be seen that the Pb-doped specimens behave like a semiconductor up to 673 K and after that further increase in the temperature results in a shifting from semiconducting to metallic behavior as inferred from the decreased electrical conductivity. The one of possible reason for this decrease in conductivity is the conversion of PbO to Pb_3O_4 at 673 K, introducing electrons to negate the predominant holes which resulted in a decreased electrical conductivity. The other reason may be the increased carrier's scattering, particularly at higher temperature, which is inferred from the increased number of grain boundaries as depicted by SEM results in Fig. 2(c). Therefore, a metallic conduction behavior was observed at higher temperature. However, further investigations are required to authenticate these propositions.

**Fig. 3.** The electrical conductivity of all the pure and doped specimens; $(\text{Ca}_{2-x}\text{M}_x\text{CoO}_3)_{0.62}(\text{CoO}_2)$; (M: Ba and Pb) as a function of temperature.

The thermal activation energy E_g for carriers can be measured from Arrhenius plots of $\ln(\sigma T)$ vs. $1000/T$ as expressed in Eq. (1) [5]:

$$\sigma = nea^2(A/T) \exp(-E_g/K_B T) \quad (1)$$

where a , e , n , A , and k_s are the inter-site distance for hopping, the charge on a carrier, the carriers concentration, the pre-exponential term related to the scattering mechanism and the Boltzmann constant, respectively. The linear relation between $\ln(\sigma T)$ and $1000/T$ suggests a small polarons hopping conduction mechanism above 573 K [19]. The activation energy E_g can be calculated from the slope of regression line, as shown in Fig. 4.

The E_g values calculated for pure and doped specimens are given in Table 2. The substitution of Ba has increased E_g and the highest E_g value of 99.13 meV was obtained by $Ba_x = 0.1$, attributed to its highest electrical conductivity. Upon further increase in the doping concentration ($x > 0.1$), the E_g value was decreased probably due to more carriers scattering with doping ions. The Pb substituted specimens has shown a decrease in E_g values due to the suppressed electrical conductivity and the lowest E_g of 55.20 meV was obtained by $Pb_x = 0.2$ owing to the suppressed transportation of carriers which is also evident from the lowest electrical conductivity of $Pb_x = 0.2$.

Thermopower power for all the series of pure and doped specimens showed positive values over the measured temperature range, indicating a p-type semiconducting behavior, as presented in Fig. 5. For all the doped specimens, thermopower was increased remarkably and for the Ba-doped specimens, a higher thermopower value of 209 $\mu V/K$ was obtained at 1000 K which was decreased upon further increase in doping concentration ($x = 0.2$). On the other hand, for Pb-doped specimens, the highest thermopower value of 225 $\mu V/K$ was obtained by $Pb_x = 0.1$ at the same temperature which was decreased slightly upon further increase in doping content. The previous report on Ba-doped CCO [25,26] and Pb-doped CCO [27] have reported no improvement in thermopower with doping. However, our results have demonstrated a remarkable enhancement in thermopower.

The enhanced thermopower can be explained on the basis of spin-entropy contribution of Co ions. The thermopower S in strongly correlated systems can be expressed by modified Heikes formula [2]:

$$S = -\frac{k_B}{e} \ln \left[\frac{g_3}{g_4} \left(\frac{c}{1-c} \right) \right] \quad (2)$$

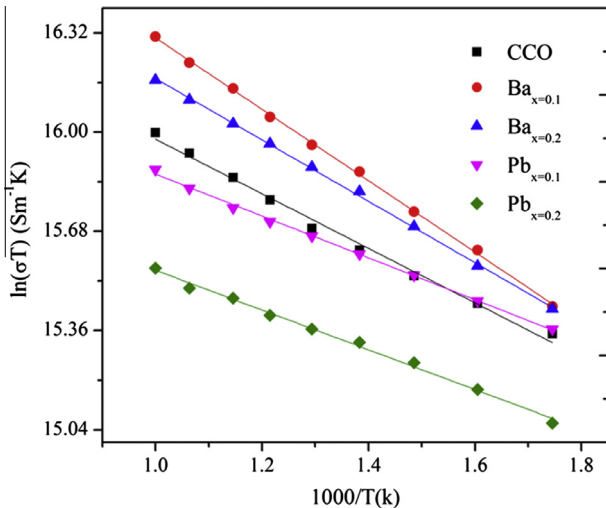


Fig. 4. The determination of activation energies for all the pure and doped specimens; $(Ca_{2-x}M_xCoO_{3})_{0.62}$ (CoO_2); (M: Ba and Pb) from Arrhenius plots.

Table 2

Relative ionic concentrations (%) of Co^{3+} and Co^{4+} determined from the high resolution Co 2p XPS spectra and the activation energies (E_g) for the pure $(Ca_2CoO_3)_{0.62}$ (CoO_2) and doped $(Ca_{1-x}M_xCoO_3)_{0.62}$ (CoO_2); (M: Ba, Pb) specimens.

| Samples | Ionic concentrations (%) | | E_a (meV) |
|--------------|--------------------------|-----------|-------------|
| | Co^{3+} | Co^{4+} | |
| CCO | 36.24 | 63.76 | 75.79 |
| $Ba_x = 0.1$ | 41.69 | 58.31 | 99.13 |
| $Ba_x = 0.2$ | 41.49 | 58.51 | 85.26 |
| $Pb_x = 0.1$ | 44.57 | 55.43 | 58.09 |
| $Pb_x = 0.2$ | 38.83 | 61.17 | 55.20 |

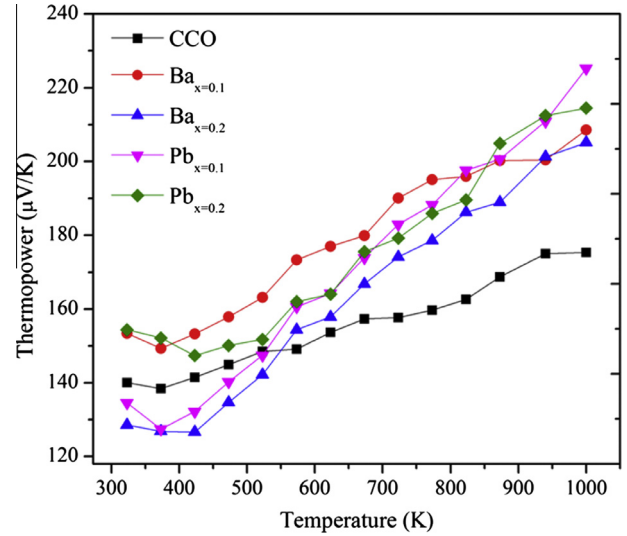


Fig. 5. Temperature dependence of thermopower for all the pure and doped specimens; $(Ca_{2-x}M_xCoO_3)_{0.62}$ (CoO_2); (M: Ba and Pb).

where e is the charge on an electron, k_B is the Boltzmann constant, g_3 and g_4 are the spin orbital degeneracies for Co^{3+} and Co^{4+} respectively and c is the concentration of Co^{4+} . Eq. (2) states that the thermopower depends implicitly upon c and any suppression in it would result in an increased spin-entropy which increases thermopower. To investigate the Ba and Pb doping effects upon the spin-entropy, XPS spectrum for Co 2p were measured. To determine the binding energies and concentrations of Co^{3+} and Co^{4+} , the high resolution Co 2p spectrum was deconvoluted with the help of synthetic peak fitting, as shown in Fig. 6. The relative concentration for each Co ion was determined by calculating the ratio of an area under the respective peak to the total area subscribed by Co 2p [17,18]. The predicted concentrations of Co^{3+} and Co^{4+} along with their binding energies are listed in Table 2. It can be noted that the Ba-doping has increased the spin-entropy by suppressing the Co^{4+} concentration, thus, a higher thermopower was obtained. For the Pb-doping, the increase in thermopower might be resulted explicitly through the suppression Co^{4+} concentration, and the carrier's concentration inferred from the decreased electrical conductivity.

The power factor: PF (σS^2) for all the pure and doped specimens as a function of temperature is presented in Fig. 7. For the Ba-doped samples, the simultaneous increase in the electrical conductivity and the thermopower increased PF. However, for the Pb-doped samples, the electrical conductivity was decreased and the thermopower was increased, thus a higher PF value of 400 $\mu W/mK^2$ at 1000 K was attained by $Pb_x = 0.1$. The highest PF value of 527 $\mu W/mK^2$ at the same temperature, among all the pure and doped specimens, has been obtained by $Ba_x = 0.1$, which is about 50% higher than that of pure CCO.

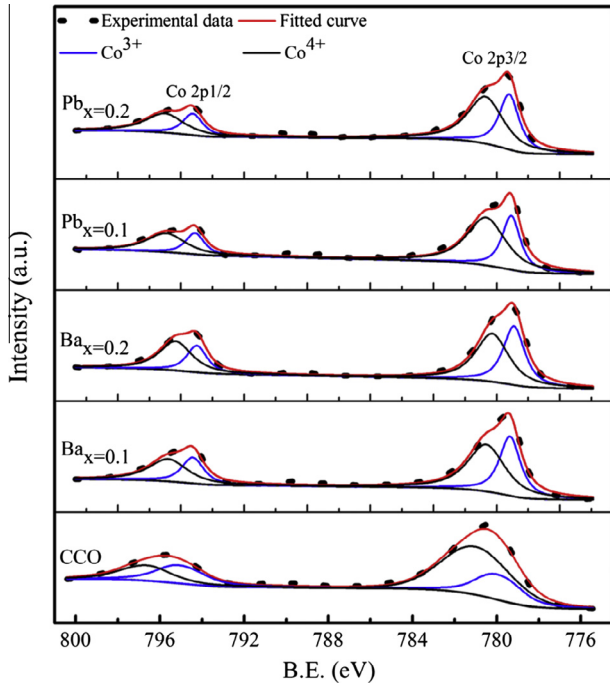


Fig. 6. High-resolution XPS spectra for Co 2p with relative concentrations of Co^{3+} and Co^{4+} .

Fig. 8 presents the temperature dependence of thermal conductivity for all the pure and doped specimens. Fig. 8(a) depicts that the total thermal conductivity k of all the specimens decreases with the increasing temperature, representing the typical thermal conduction behavior in crystalline semiconductors, which indicates that the total thermal conductivity is mainly composed of phonon thermal conduction [21]. It can be seen that Ba- and Pb-doping has decreased the total thermal conductivity because of the increased phonons scattering from heavy-metal ions i.e.; Ba^{2+} and Pb^{2+} , as shown in Fig. 8(b).

The total thermal conductivity k can be expressed as $k = k_{ph} + k_{hole}$, where k_{ph} and k_{hole} are the thermal conductivities associated with the phonon and hole transportation, respectively. k_{hole} can be estimated from Wiedemann–Franz law, viz. $k_{hole} = L_0 \sigma T$, where $L_0 = \pi^2 k_B^2 / 3e^2$ is the Lorentz constant and σ is the electrical

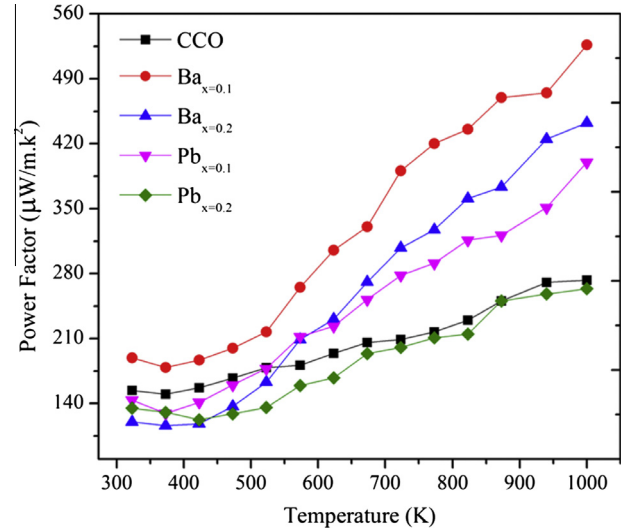


Fig. 7. Temperature dependence of the power factor for all the pure and doped series: $(\text{Ca}_{2-x}\text{M}_x\text{CoO}_3)_{0.62}$ (CoO_2); (M: Ba and Pb).

conductivity [5]. All the doped specimens showed a noticeable reduction in thermal conductivity mainly because of the increased phonon scattering. However, the total thermal conductivity belonging to $\text{Ba}_{x=0.1}$ is comparable to that of the CCO because the decrease in k caused by the suppressed k_{ph} is compensated by the increased k_{hole} , as shown in Fig. 8(c). For Pb-doped specimens, an evident decrease in the thermal conductivity can be observed because of its relatively higher atomic mass leading to higher phonon scatter which results in a decreased thermal conductivity. For all the Ba- and Pb-doped specimens, the thermal conductivity was decreased upon further increase in doping concentrations because of increased scattering sites for phonons. It can be observed clearly in Fig. 8(a) that among all the pure and doped specimens, the lowest k value of 1.39 W/m K at 1000 K belonged to $\text{Pb}_{x=0.2}$, which resulted from the simultaneous decrease in k_{ph} and k_{hole} , as manifested by Fig. 8(b and c).

The dimensionless figure of merit ZT is calculated from PF and the total thermal conductivity. Fig. 9 depicts that the ZT value for all the pure and doped series increases monotonically with the increasing temperature. The ZT for all the doped specimens is higher than that of CCO. With Pb-doping, a higher ZT value of ~ 0.27 at

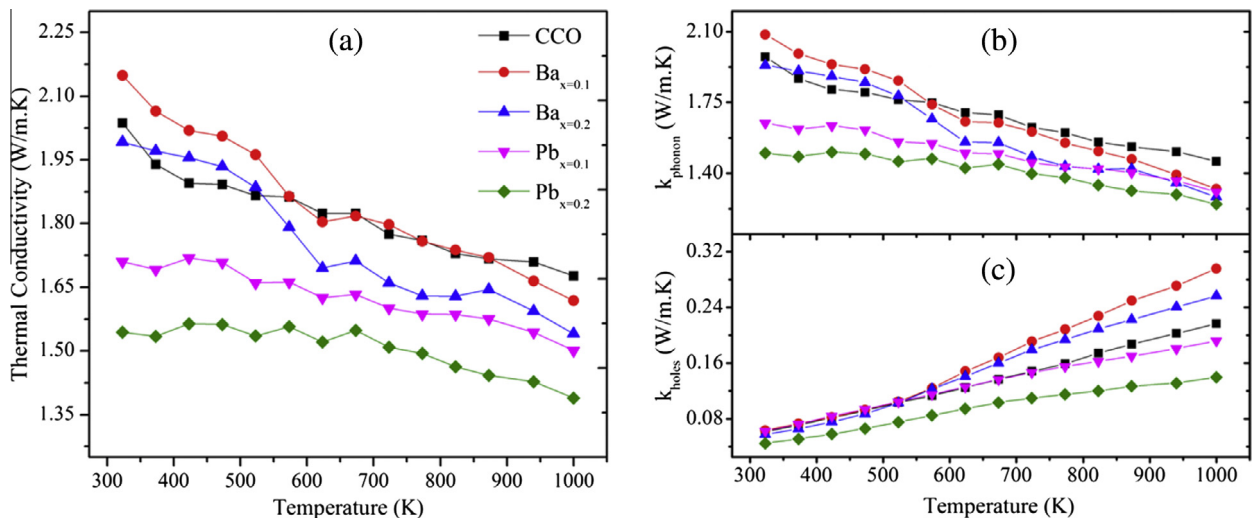


Fig. 8. Temperature dependence of (a) total thermal conductivity, (b) the phonon thermal conductivity and (c) the hole thermal conductivity.

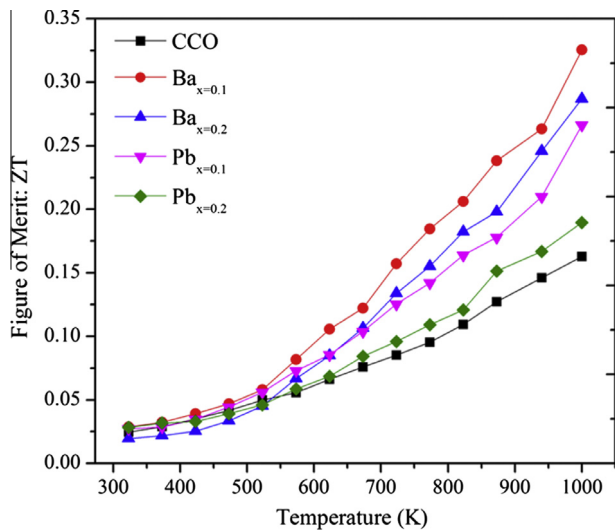


Fig. 9. Dimensionless figure of merit: ZT as a function of temperature for all the series of pure and doped ceramics: $(\text{Ca}_{2-x}\text{M}_x\text{CoO}_3)_{0.62}$ (CoO_2); (M: Ba and Pb).

1000 K, was obtained by $\text{Pb}_{x=0.1}$. The highest ZT value of ~ 0.33 belonging to $\text{Ba}_{x=0.1}$ at 1000 K has been achieved, which is even higher than that of reported in Ref. [25] for Ba-doped CCO.

4. Conclusions

A series of Ba-doped $(\text{Ca}_{2-x}\text{Ba}_x\text{CoO}_3)_{0.62}$ (CoO_2) and Pb-doped $(\text{Ca}_{2-x}\text{Pb}_x\text{CoO}_3)_{0.62}$ (CoO_2); ($x = 0, 0.1, 0.2$) ceramics has been prepared by sol-gel method followed by SPS. The partial substitution of Ba at Ca-site has increased the electrical conductivity but the Pb doping has suppressed the electrical conductivity. For all the pure and doped specimens, the small polarons hopping conduction mechanism was observed above 573 K. It was found that the bivalent metallic-doping induced a spin-entropy, which resulted in an enhanced thermopower. The highest power factor was obtained by $\text{Ba}_{x=0.1}$ through simultaneously increase in the electrical conductivity and thermopower. At the same time, Ba-doping suppressed the thermal conductivity, which resulted in an increased ZT value. On the other hand, the partial substitution of Pb at Ca-site decreased the electrical conductivity and increased the thermopower but the later prevailed upon former, which led to a higher power factor. The lowest thermal conductivity was obtained with Pb-doping because of its heavier atomic mass, which resulted in a higher ZT value of ~ 0.27 . Among all the pure and doped series, the highest ZT value of ~ 0.33 at 1000 K was achieved by Ba-doping, which was about 100% higher than that of pure CCO. This promising improvement in ZT with Ba-doping makes CCO a potential candidate for p-type thermoelectric materials to be used for high temperature applications.

Acknowledgements

This work was financially supported by NSF of China (Grant No. 51221291) and the Ministry of Sci. & Tech. of China through a 973-Project, (Grant No. 2013CB32506). The authors are thankful to Mr. Rao Nauman Naseem of Tsinghua University, Beijing, for the useful discussion with him.

References

[1] Hochbaum AI, Chen R, Delgado RD, Liang W, Garnett EC, Najarian M, et al. Enhanced thermoelectric performance of rough silicon and nanowires. *Nature* 2008;451:163–7.

[2] Karri MA, Thacher EF, Helenbrook BT. Exhaust energy conversion by thermoelectric generator: two case studies. *Energy Convers Manage* 2011;52:1596–611.

[3] Hadjistassou C, Kyriakides E, Georgiou J. Designing high efficiency segmented thermoelectric generators. *Energy Convers Manage* 2013;66:165–72.

[4] Choi SM, Lee KH, Lima CH, Seo WS. Oxide-based thermoelectric power generation module using p-type $\text{Ca}_3\text{Co}_4\text{O}_9$ and n-type $(\text{ZnO})_7\text{In}_2\text{O}_3$ legs. *Energy Convers Manage* 2011;52:335–9.

[5] Nolas GS, Sharp J, Goldsmid HJ. *Thermoelectrics: basic principles and new materials developments*. New York: Springer; 2001.

[6] Liu Y, Zhao LD, Liu Y, Lan J, Xu W, Li F, et al. Remarkable enhancement in thermoelectric performance of BiCuSeO by Cu deficiencies. *J Am Chem Soc* 2011;133:20112–5.

[7] Sui J, Li J, He J, Pei YL, Berardan D, Wu H, et al. Texturation boosts the thermoelectric performance of BiCuSeO oxytellurides. *Energy Environ Sci* 2013;6:2916.

[8] Terasaki I, Sasago Y, Uchinokura K. Large thermoelectric power of NaCo_2O_4 single crystals. *Phys Rev B* 1997;56:12685–7.

[9] Masset AC, Michel C, Maignan A. Misfit-layered cobaltite with an anisotropic giant magnetoresistance: $\text{Ca}_3\text{Co}_4\text{O}_9$. *Phys Rev B* 2000;62:166.

[10] Funahashi R, Matsubara I, Sodeoka S. Thermoelectric properties of $\text{Bi}_2\text{Sr}_2\text{Co}_2\text{O}_x$ polycrystalline materials. *Appl Phys Lett* 2000;76:2385.

[11] Wang Y, Xu L, Sui Y, Wang X, Cheng J, Su W. Enhanced electron correlation in rare-earth doped $\text{Ca}_3\text{Co}_4\text{O}_9$. *Appl Phys Lett* 2010;97:062114.

[12] Ngo NV, Nini P, Søren L, Michitaka O. Enhancement of the thermoelectric performance of p-type layered oxide $\text{Ca}_3\text{Co}_4\text{O}_{9+\delta}$ through heavy doping and metallic nano-inclusions. *Adv Mater* 2011;23:2484–90.

[13] Koshibae W, Maekawa S. Effect of spin and orbital on thermopower in strongly correlated electron systems. *J Magn Magn Mater* 2003;258:216–8.

[14] Shikano M, Funahashi R. Electrical and thermal properties of single-crystalline $(\text{Ca}_2\text{CoO}_3)_{0.7}\text{CoO}_2$ with a $\text{Ca}_3\text{Co}_4\text{O}_9$ structure. *Appl Phys Lett* 2003;82:1851–3.

[15] Li S, Funahashi R, Matsubara I, Ueno K, Sodeoka S, Yamada H. Synthesis and thermoelectric properties of the new oxide materials $\text{Ca}_{3-x}\text{Bi}_x\text{Co}_4\text{O}_{9+\delta}$ ($0.0 < x < 0.75$). *Chem Mater* 2000;12:2424–7.

[16] Xu G, Funahashi R, Shikano M, Matsubara I, Zhou Y. Thermoelectric properties of the Bi- and Na-substituted $\text{Ca}_3\text{Co}_4\text{O}_9$ system. *Appl Phys Lett* 2008;93:3760.

[17] Tang GD, Wang ZH, Xu XN, Qiu L, Du YW. Evidence of spin density-wave transition and enhanced thermoelectric properties in $\text{Ca}_{3-x}\text{Ce}_x\text{Co}_4\text{O}_{9+\delta}$. *J Appl Phys* 2010;107:053715.

[18] Song Y, Nan CW. High temperature transport properties of Ag-added $(\text{Ca}_{0.975}\text{La}_{0.025})_3\text{Co}_4\text{O}_9$ ceramics. *Physica B* 2011;406:2919–23.

[19] Lin YH, Nan CW, Liu Y, Li JF, Mizokawa T, Shen Z. High-temperature electrical transport and thermoelectric power of partially substituted Ca_3CaO_9 -based ceramics. *J Am Ceram Soc* 2007;90:132–6.

[20] Zhang FP, Zhang X, Lu QM, Zhang JX, Liu YQ, Zhang GZ. Preparation and high temperature thermoelectric properties of $\text{Ca}_{3-x}\text{Ag}_x\text{Co}_4\text{O}_{9+\delta}$ oxides. *Solid State Sci* 2011;13:1443–7.

[21] Constantinescu G, Rasekh S, Torres MA, Diez JC, Madre MA, Sotelo A. Effect of Sr substitution for Ca on the $\text{Ca}_3\text{Co}_4\text{O}_9$ thermoelectric properties. *J Alloys Compd* 2013;577:511–5.

[22] Lee WG, Kim JY, Athar T, Kim SJ, Seo WS, Park K. Electrical conductivity and thermoelectric power studies of solution-combustion-processed $\text{Ca}_{2.76}\text{Cu}_{0.24}\text{Co}_4\text{O}_9$. *Ceram Int* 2013;39:1397–402.

[23] Bhaskar A, Lin ZR, Liu CJ. Thermoelectric properties of $\text{Ca}_{2.95}\text{Bi}_{0.05}\text{Co}_{4-x}\text{Fe}_x\text{O}_{9+\delta}$ ($0 \leq x \leq 0.15$). *Energy Convers. Manage.* 2013;76:63–7.

[24] Bhaskar A, Lin ZR, Liu CJ. Thermoelectric properties of $\text{Ca}_{3-x}\text{Eu}_x\text{Co}_4\text{O}_{9+\delta}$ ($0 \leq x \leq 0.1$). *Solid State Commun* 2013;168:24–7.

[25] Zhang F, Lu Q, Li T, Zhang X, Zhang J, Song X. Preparation and thermoelectric transport properties of Ba-, La- and Ag-doped $\text{Ca}_3\text{Co}_4\text{O}_9$ oxide materials. *J Rare Earths* 2013;31:8.

[26] Lu QM, Zhang JX, Zhang QY, Liu YQ, Liu DM. Improved thermoelectric properties of $\text{Ca}_{3-x}\text{Ba}_x\text{Co}_4\text{O}_9$ ($x = 0-0.4$) bulks by sol-gel and SPS method. *IEEE* 2006;1-4244:0811–3.

[27] Nakatsugawa H, Jeong HM, Kim RH, Gomi N. Thermoelectric and magnetic properties of $[(\text{Ca}_{1-x}\text{Pb}_x)_2\text{CoO}_{3.1}]_{0.62}\text{CoO}_2$ ($0 \leq x \leq 0.03$). *Jpn J Appl Phys* 2007;46:5.

[28] Huang Y, Zhao B, Ang R, Lin S, Huang Z, Tan S, et al. Enhanced thermoelectric performance and room-temperature spin-state transition of Co^{4+} ions in the $\text{Ca}_3\text{Co}_{4-x}\text{Rh}_x\text{O}_9$ system. *J Phys Chem C* 2013;117:11459–70.

[29] Tian R, Donelson R, Ling CD, Blanchard PER, Zhang T, Chu D, et al. Ga substitution and oxygen diffusion kinetics in $\text{Ca}_3\text{Co}_4\text{O}_{9+\delta}$ -based thermoelectric oxides. *J Phys Chem C* 2013;117:13382–7.

[30] Pinitsoontorn S, Lersongkram N, Keawprak N, Amornkitbamrung V. Thermoelectric properties of transition metals-doped $\text{Ca}_3\text{Co}_{3.8}\text{M}_{0.2}\text{O}_{9+\delta}$ (M: Co, Cr, Fe, Ni, Cu and Zn). *J Mater Sci* 2012;23:1050–6.

[31] Wang Y, Sui Y, Ren P, Wang L, Wang X, Su W, et al. Strongly correlated properties and enhanced thermoelectric response in $\text{Ca}_3\text{Co}_{4-x}\text{M}_x\text{O}_9$ (M = Fe, Mn, and Cu). *Chem Mater* 2010;22:1155–63.

[32] Wang Y, Sui Y, Wang X, Su W, Liu X. Enhanced high temperature thermoelectric characteristics of transition metals doped $\text{Ca}_3\text{Co}_4\text{O}_{9+\delta}$ by cold high-pressure fabrication. *J Appl Phys* 2010;107:033708.

[33] Yao Q, Wang DL, Chen LD, Shi X, Zhou M. Effects of partial substitution of transition metals for cobalt on the high-temperature thermoelectric properties of $\text{Ca}_3\text{Co}_4\text{O}_{9+\delta}$. *J Appl Phys* 2005;97:103905.

- [34] Butt S, Liu YC, Lan JL, Shehzad K, Zhan B, Lin Y, et al. High-temperature thermoelectric properties of La and Fe co-doped Ca–Co–O misfit-layered cobaltites consolidated by spark plasma sintering. *J Alloys Compd* 2014;588:277–83.
- [35] Ou Y, Peng J, Li F, Yu ZX, Ma FY, Xie SH, et al. The effects of dual doping on the thermoelectric properties of $\text{Ca}_{3-x}\text{M}_x\text{Co}_{4-y}\text{Cu}_y\text{O}_9$ (M = Na, La). *J Alloys Compd* 2012;526:139–44.
- [36] Hao HS, Zhao LM, Hu X. Microstructure and thermoelectric properties of Bi- and Cu-substituted $\text{Ca}_3\text{Co}_4\text{O}_9$ oxides. *J Mater Sci Technol* 2009;25:105.
- [37] Liu Y, Lin Y, Shi Z, Nan CW. Preparation of $\text{Ca}_3\text{Co}_4\text{O}_9$ and Improvement of its thermoelectric properties by spark plasma sintering. *J Am Ceram Soc* 2005;88:1337–40.